Journal of Photopolymer Science and Technology
Volume 29, Number 5 (2016) 709－715 ©2016SPST

Direct Self-Assembly for Non-Periodic Designs

**Kenji Yoshimoto*[a, b], Akihisa Yoshida[a], Masahiro Ohshima[a]
Katsuyoshi Kodera[c], Yoshihiro Naka[c], Hideki Kanai[c], Sachiko Kobayashi[c], Simon Maeda[c],
Phubes Jiravanichsakul[c], Katsutoshi Kobayashi[c], and Hisako Aoyama[c]**

*[a]Dept. of Chemical Engineering, Graduate School of Engineering, Kyoto Univ., Japan;
[b]Center for the Promotion of Interdisciplinary Education and Research, Kyoto Univ., Japan;
[c] Memory Technology Research & Development Center, Toshiba Corporation
yoshimoto1@cheme.kyoto-u.ac.jp

Previously we investigated a directed self-assembly (DSA) process for fabricating a non-periodic pattern (i.e., wide line) lying in between the periodic line/space patterns. A symmetric poly(styrene-*block*-methyl methacrylate) (PS-*b*-PMMA) was employed here, which formed a lamella morphology with the natural period (L_0) of 30 nm. Unlike the conventional DSA process, we used ArF resist patterns as the chemical guides, and generated a horizontal lamella on the non-periodic guide pattern as an etch template for fabricating the wide line. Our preliminary results showed that controlling the morphological defects around the boundary between the periodic and non-periodic regions would be crucial for this DSA flow. In this paper, we report on how the width of the non-periodic pattern, W, would affect on the overall self-assembled morphology of PS-*b*-PMMA on the pre-patterned surface. The experimental results showed that a transition from the perpendicular to horizontal lamella on the non-periodic pattern occurred at W=2.50 L_0. It was also revealed from our simulations that at W=1.50 L_0, the perpendicular PS-rich domain was not attached to the guide surface; it might be taken off after the removal of PMMA. For W>3.5 L_0, the wide line was transferred to the underlying silicon (Si) substrate, but some large defects were observed in the non-periodic region, possibly due to some residues of the neutral materials on top of the ArF guide pattern.
Keywords: directed self-assembly, diblock copolymer, PS-b-PMMA, lamella, non-periodic, simulation

1. Introduction

A diblock copolymer consists of the two chemically different polymer chains ("blocks"). If the one block strongly repulses the other, the diblock copolymers spontaneously assemble a periodic structure with the pitch, L_0, of a few tens of nanometers. The directed self-assembly (DSA) of the diblock copolymers utilizes a chemically or physically pre-patterned surface to control the orientation and position of the self-assembled domains [1]. The DSA may be a simple, cost-effective patterning approach for fabricating very fine patterns (e.g., half pitch of ~15-20 nm), but it still needs to improve the defect level and the placement error for high-volume manufacturing of semiconductor devices [2,3].

Another challenge for the DSA, which we focus in this study, is to generate patterns of different sizes and pitches that are relevant to a circuit design. A conventional approach to include non-periodic features in the periodic DSA patterns is the use of cut/block masks. For example, the silicon fins required for the FinFET device have been fabricated by cutting the DSA lamellae into groups of line segments [4-6]. Recently, Doerk et al. have demonstrated a new DSA flow for fabricating an arbitrary design of patterns without the cutting process (Fig. 1) [7,8]. In their flow, a hydrogen silsesquioxane (HSQ) was used to generate the guiding and masking features (Fig.

Received May 15, 2016
Accepted June 3, 2016

1a). During spin-coating and annealing of a symmetric poly(styrene-*block*-methyl methacrylate) (PS-*b*-PMMA) on the pre-patterned surface, the PMMA-rich lamella domains were preferentially formed on the HSQ guiding patterns (Fig. 1b). The self-assembled morphology of the PS-*b*-PMMA on the HSQ masking features should ideally be perpendicular lamella to the substrate, and be aligned with the ones in the periodic regions. This was mainly to eliminate a formation of morphological defects at the boundary between the periodic and non-periodic regions. Consequently, the width of the non-periodic pattern (i.e., masking feature) was limited up to a few L_0. After the removal of the PMMA domains (Fig. 1c), the remaining PS and HSQ patterns were used as an etch template that protects the underlying layers from reactive ion etching (RIE) (Fig. 1d). Note that not only the masking but also guiding HSQ patterns were not transferred to the substrate due to a high etch resistivity of the HSQ; the pitch of the guide patterns in the periodic regions became bimodal (i.e., 1 L_0 and 2 L_0).

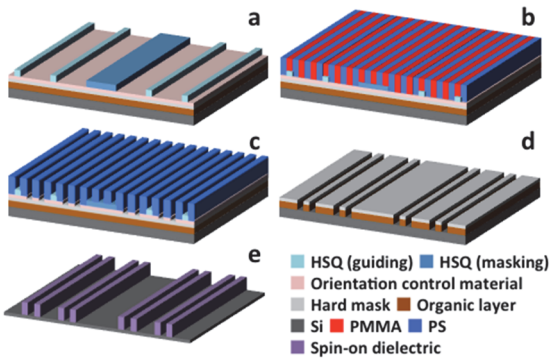

Fig. 1. (Color online) Schematic DSA process flow proposed by Doerk et al. [7]: (a) Pre-patterned surface with the HSQ features. (b) Annealing of symmetric PS-*b*-PMMA. (c) PMMA removal. (d) Pattern transfer to the underlying layers through the composite (PS and HSQ) mask. (e) Pattern tone inversion.

In our previous work, we demonstrated an alternative DSA patterning that may include non-periodic patterns between the globally aligned DSA lamellae, by using a relatively simple and cost-effective approach [11]. The non-periodic pattern here indicates a wide line lying between the two periodic blocks of 1:1 line and space patterns with the pitch of 1 L_0 (~30 nm). Various sizes of the wide lines are demanded for memory and logic devices. Although the use of the cut/block masks is a standard approach to fabricate such wide lines, it may increase the cost and need an extremely accurate control for placing the edges of the cut/block patterns in between the narrow spaces (~15 nm) [4-6].

Our DSA flow is illustrated in Fig. 2 (see Section 2.1 for the details). A major difference from the approach of Doerk et al. is that we used an ArF resist for the guide patterns [9,10]. Unlike the HSQ, the ArF resist can easily be removed by etching; the remaining PS domains after the PMMA removal play an essential role as a resist. Also, we generated a horizontal lamella (or a horizontally oriented PS domain) on the non-periodic guide pattern to use it as an etch template for fabricating the wide line [11]. Advantages of our DSA flow are that we can use the same resist and processes which have already been implemented in the 193 nm immersion lithography, and that we may fabricate various widths of the non-periodic patterns without using cut/block masks.

In this paper, we report on some effects of the design of non-periodic pattern on the self-assembled morphology of PS-*b*-PMMA. There are two important design parameters for the non-periodic patterns: the width of the non-periodic pattern, W, and the space between the periodic and non-periodic guide patterns, S (previously denoted by $S1$ and $W1$ in Ref. [11], respectively). In our previous experiments, the results suggested that the S match with the space in the periodic regions, i.e., ~2.5 L_0, to minimize the formation of morphological defects [11]. Therefore, we focused on investigating how the W would affect on the self-assembled morphology of the symmetric PS-*b*-PMMA on the non-periodic pattern. The experiments were conducted by the same procedures as described in Ref. [11]. The morphology of the self-assembled PS-*b*-PMMA on the pre-patterned surface was characterized by the scanning electron microscope (SEM). We also performed the simulations to provide insights into the morphology of the self-assembled PS-*b*-PMMA in three dimensions.

2. Methods

2.1. Experiments

For brevity, we describe only the key steps of our DSA flow (Fig. 2). Further details can be found elsewhere in Refs. [9-11].

i) Lithographic patterning of ArF resist

An ArF resist was spin-coated on the 300 mm silicon wafer covered with spin-on-glass (SOG) and spin-on-carbon (SOC) layers. Then the ArF resist film was fabricated into the periodic and non-periodic patterns by 193 nm immersion lithography. The width and pitch of the resist patterns in the periodic regions were 45 nm and 90 nm, respectively.

ii) Etching of the ArF resist patterns

The ArF resist patterns were transferred to the underlying SOG layer by RIE. This etch process was stopped when the width of the ArF periodic patterns became ~15 nm. Importantly, a thin ArF resist was kept on the top surface of the SOG features.

iii) Filling the spaces with neutral materials

Neutral materials composed of random copolymers were spin-coated and annealed on the patterned surface. Since the neutral materials were designed to graft not to the ArF resist but to the SOG, only the spaces between the guide patterns were covered with the neutral brush. After rising the non-grafted random copolymers, the height of the guide patterns became ~10 nm from the top surface of the neutral layer [11].

iv) DSA of lamella-forming PS-b-PMMA

A symmetric PS-*b*-PMMA (30 kg/mol for PS and 30 kg/mol for PMMA, L_0 = ~30 nm) was spin-coated on the pre-patterned surface and annealed at 250 ℃ for 2 minutes. The film thickness of the PS-*b*-PMMA was set at ~38 nm (~1.3 L_0) to stably form the perpendicular lamellae in the periodic regions [11]. After annealing, the PMMA domains were preferentially located on the top surface (i.e., ArF resist) of the guide patterns due to a high affinity between the PMMA and ArF resist.

v) PMMA removal and pattern transfer

The PMMA domains were removed by etching, and the remaining PS patterns were used as a template for the pattern transfer to the underlying hardmasks.

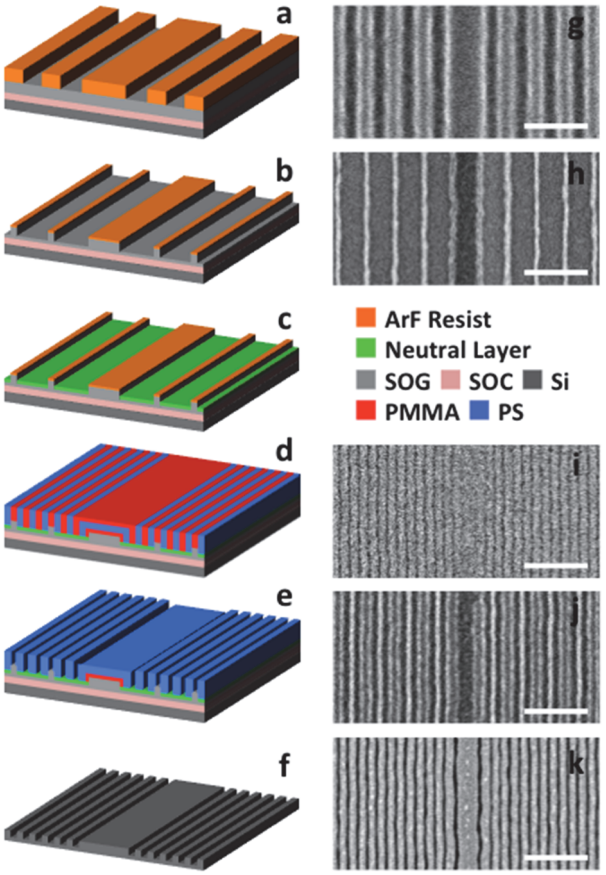

Fig. 2. (Color online) DSA process flow for creating periodic and non-periodic patterns with ArF resist: (left) schematic illustrations and (right) top-down SEM images. (a,g) Periodic and non-periodic patterns of ArF resist. (b,h) Pattern transfer to the underlying SOG layer. (c) Grafting the neutral layer. (d,i) Annealing of the symmetric PS-*b*-PMMA. (e, j) PMMA removal. (f, k) Final pattern transfer to Si substrate.

2.2. Simulations

In order to simulate a self-assembled morphology of the symmetric PS-*b*-PMMA on the pre-patterned substrate, we used the Ohta-Kawasaki (OK) model [12], whose details can be found in Ref. [13]. In the OK model, the melt of *AB* diblock copolymers is assumed to be incompressive; sum of the local volume fraction of block *A* (= PMMA), $\phi_A(\boldsymbol{r})$, and that of block *B* (= PS), $\phi_B(\boldsymbol{r})$, becomes unity at a given position $\boldsymbol{r}$. The difference in the volume fractions between the two blocks, $\phi_A(\boldsymbol{r}) - \phi_B(\boldsymbol{r})$, is defined as an order parameter, $\eta(\boldsymbol{r})$. The total free energy of the system, *F*, is expressed as a function of $\eta(\boldsymbol{r})$;

$$F\{\eta(\boldsymbol{r})\} = \int dr\,(f_b + f_s). \quad (1)$$

The bulk energy term, f_b, is given by

$$f_b = -\frac{1}{2\xi^2}\ \eta(\boldsymbol{r})^2 + \frac{g}{4}\eta(\boldsymbol{r})^4 + \frac{1}{2}\ [\nabla\eta(\boldsymbol{r})]^2 + \frac{\alpha}{2}\ \int d\boldsymbol{r}'\, G(\boldsymbol{r},\boldsymbol{r}')[\eta(\boldsymbol{r}) - \bar{\eta}][\eta(\boldsymbol{r}') - \bar{\eta}], \quad (2)$$

where $G(\boldsymbol{r},\boldsymbol{r}')$ is the Green function and $\bar{\eta}$ is the bulk average of $\eta(\boldsymbol{r})$. The coefficients ξ and α can be calculated from the block fraction and the repulsive strength, and g is a fitting parameter [12]. In this study, we used the same parameters as in Refs. [11,13].

For the surface energy term, f_s, we employed a quadratic function to control the $\phi_A(\boldsymbol{r})$ on top of the guide patterns [14];

$$f_s = \Lambda(\boldsymbol{r})[\phi_A(\boldsymbol{r}) - \ \phi_{AS}]^2, \quad (3)$$

where $\Lambda(\boldsymbol{r})$ represents a position-dependent interactive strength between the guides and the diblock copolymers; $\Lambda(\boldsymbol{r}) = \Lambda_s\ (> 0)$ on top of the PMMA-attractive guide patterns, and zero elsewhere. The other parameter, ϕ_{AS}, denotes the volume fraction of block *A* on top of the PMMA-attractive guide patterns. In the same way as in Ref. [14], we fixed Λ_s at 100, and used ϕ_{AS} as a fitting parameter to the experimental data (see Section 3.2 for the details). By using Eq. (3), the *A*–rich (= PMMA-rich) domains were pinned on top of the PMMA-attractive guide patterns more stably than the other type of the surface energy term, i.e., $f_s = \Lambda(\boldsymbol{r})\eta(\boldsymbol{r})$, which was used in our preliminary work [11].

To match with the experimental setting, the width and pitch of the guide patterns in the periodic regions were set at 0.50 L_0 (≈15 nm) and 3.00 L_0 (≈90 nm), respectively (Figs. 3a and 3c). The height of the guide patterns was adjusted from the experimental value, i.e., 0.33 L_0 (≈10 nm), to 0.19 L_0 (≈6 nm) to stabilize the perpendicular lamellae in the periodic regions [11]. The space between the nearest edges of the periodic and non-periodic guides, *S*, was fixed at 2.50 L_0 (≈75 nm), whereas the width of the non-periodic pattern, *W*, was varied from 0.50 L_0 (≈15 nm) to 3.50 L_0 (≈90 nm). The film thickness of the block copolymers was set at 1.25 L_0 (≈38 nm).

The simulations were implemented as follows. 1) A thin film of the symmetric *AB* diblock copolymers was gridded into small cubic elements with the length of 0.06 L_0 (≈2 nm). 2) A random number between 0.497 and 0.503 was assigned to each cube as an initial $\phi_A(\boldsymbol{r})$. 3) The $\phi_A(\boldsymbol{r})$ was iteratively updated by numerically solving the time-dependent Ginzburg Landau equation. In the numerical calculations, the periodic boundary conditions were applied to the *x* and *y* directions, and the hard-wall boundary condition in the *z* direction (see Ref. [13] for further details of the numerical procedures). 4) After a few million time steps, the symmetric *AB* diblock copolymers were micro-phase-separated into the *A*-rich and *B*-rich domains, including the perpendicular lamellae in the periodic regions and the horizontal lamella on the non-periodic pattern (Figs. 3b and 3d).

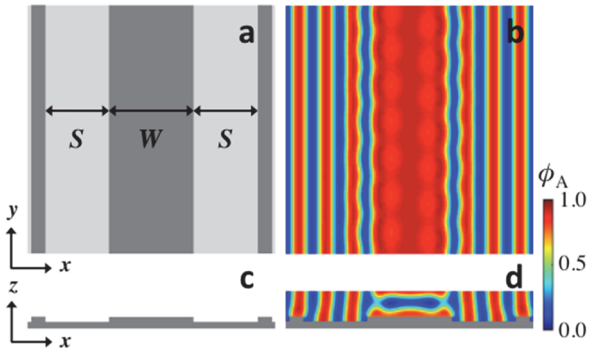

Fig. 3. (Color online) (a,c) Topology of the pre-patterned surface (*W*=3.5 L_0), and (b,d) the self-assembled morphology of the symmetric *AB* diblock copolymers obtained from the simulation. The top-down and cross-sectional images are shown at the top and bottom, respectively. In Figs. 3b and 3d, the color represents the value of $\phi_A(\boldsymbol{r})$: red for the *A*-rich (or PMMA-rich) domains and blue for the *B*-rich (or PS-rich) domains, respectively.

3. Results and Discussion

3.1. Experimental Results

Figure 4 illustrates the top-down SEM images with four different widths of the non-periodic pattern, which were taken after the final pattern transfer to the Si substrate (Figs. 1f and 1k). In all cases, the space between the periodic and non-periodic regions, *S*, was fixed at 2.50 L_0 (75 nm). At *W*=0.50 L_0 (15 nm), the non-periodic pattern became the regular guide patterns; 1:1 line and space patterns with the pitch of 1.00 L_0 (30 nm) were perfectly aligned on the pre-patterned surface (Fig. 4a). Interestingly, the non-periodic pattern was transferred as a space at *W*=1.50 L_0 (45 nm) (Fig. 4b), not as a wide line observed at $W \geq 2.50\ L_0$ (Figs. 4c and 4d). This reason will be explained by using the simulation results in Sec. 3.3.

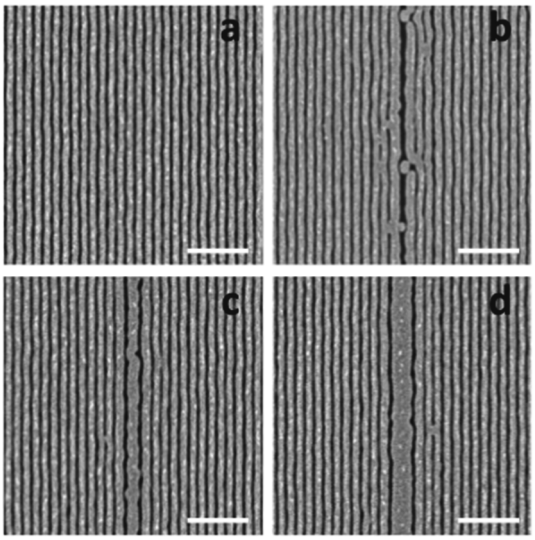

Fig. 4. Effect of the width of the non-periodic pattern on the self-assembled morphology of symmetric PS-*b*-PMMA (L_0≈30 nm): (a) W = 0.5 L_0, (b) 1.5 L_0, (c) 2.5 L_0, and (d) 3.5 L_0. All the top-down SEM images were taken after the final pattern transfer to the Si substrate. The line and space patterns are shown by gray and black colors, respectively. The scale bar (white line) is 200 nm.

3.2. Calibration of Model Parameter

In order to see if we could capture the similar morphological changes as observed in the experiments (Fig. 4) by simulations, we varied the model parameter in Eq. (3), ϕ_{AS}, from 0.6 to 0.8 (Fig. 5). The ϕ_{AS} represents the volume fraction of block *A* (=PMMA) on top of the PMMA-attractive guide patterns; as the ϕ_{AS} becomes larger, the more *A*-rich domains are attached on top of the guide patterns. It is shown in Figs. 5a-5c that ϕ_{AS}=0.6 was not large enough to attract the *A*-rich domains to the guide surface, and therefore that the perpendicular lamellae formed defects anywhere on the pre-patterned surface. By increasing ϕ_{AS} from 0.6 to 0.7, not only the *A*-rich domains in the periodic regions were tightly pinned on the guide patterns, but also the horizontal lamella was formed on top of the non-periodic patterns at W≥2.50 L_0 (Figs. 5d-5f). This threshold of W roughly matched with the experimental data (Fig. 4). On the other hand, it was found that the attractive strength of the guide patterns became too strong at ϕ_{AS}=0.8 (Figs. 5g-5i). For example, the horizontal lamella was generated on the non-periodic pattern at W=1.50 L_0, which was smaller by ~1.00 L_0 than the experiments (~2.50 L_0). Based on these results, we set ϕ_{AS}=0.7 for the following simulations.

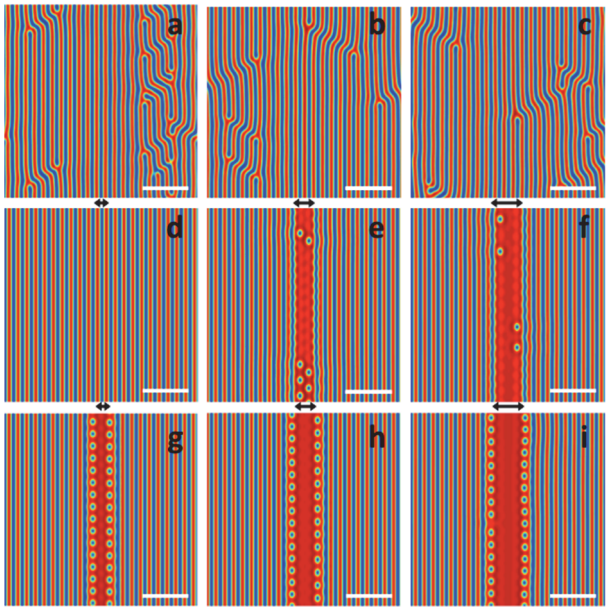

Fig. 5. (Color online) Morphological changes with the model parameter, ϕ_{AS}: (a,b,c) ϕ_{AS}=0.6, (d,e,f) 0.7, and (g,h,i) 0.8. For each ϕ_{AS}, the self-assembled morphologies at three different widths of the non-periodic pattern were simulated: (left) W = 1.5 L_0, (middle) 2.5 L_0, and (right) 3.5 L_0. The size of W is denoted by the double-sided arrow. The same coloring was used as in Fig. 3; the *A*-rich and *B*-rich domains are shown by red and blue colors, respectively. The scale bar (white line) is ~6.7 L_0 (~200 nm).

3.3. Simulation Results

Figure 6 summarizes our simulation results, showing how the self-assembled morphology of the symmetric *AB* diblock copolymers is changed with the width of the non-periodic pattern, W. In all these simulations, the ϕ_{AS} was fixed at 0.7. At W=1.5 L_0, the perpendicular lamellae were formed on the non-periodic pattern, and the *B*-rich (=PS-rich) domain was sandwiched between the two *A*-rich (=PMMA-rich) domains (Fig. 6b). Interestingly, the two *A*-rich domains were connected at the bottom. In such a configuration, the B-rich domain may be taken off partially or entirely from top of the non-periodic pattern after removal of the A-rich domains. This may explain why the space was observed in the non-periodic region of W=1.5 L_0 after the final pattern transfer to the Si substrate (Fig. 4b). As the W was increased to 2.50 L_0, the orientation of the lamella on the non-periodic pattern was changed from "perpendicular" to "horizontal" to the substrate (Fig. 6c). The horizontal lamella was always observed on the non-periodic pattern at W≥2.50 L_0 (Fig. 6d). This implies that the horizontal lamella may be

energetically stable at $W \geq 2.50\ L_0$ due to a large enthalpic gain by the attractive interactions between the *A*-rich domains and the top surface of the non-periodic pattern. Also, at $W \geq 2.50\ L_0$, the *B*-rich domain in the non-periodic region becomes *H*-shape after the removal of *A*-rich domains. Whether such an irregular-shape *B*-rich domain would be real and transferable to the underlying layers will need to be further investigated.

Overall, the simulation results (Figs. 5d-5f and Fig. 6) have a reasonable agreement with the experimental data (Fig. 4). Note, however, that some defect morphologies were observed in the experiments. For example, some large defects were formed in the non-periodic region at $W > 3.50\ L_0$ (Fig. 7). Those defects were composed of the perpendicular lamellae and transferred to the underlying layer. It is speculated that the top surface (i.e., ArF resist) of the non-periodic pattern might be partially covered with the neutral materials. Another common type of the defects found in the experiments is a large dislocation of the perpendicular lamellae located around the boundary between the periodic and non-periodic regions (see Fig. 7b for example). It is believed that the edge roughness and slope of the non-periodic pattern might have some non-trivial effects on the self-assembled morphology of the PS-*b*-PMMA.

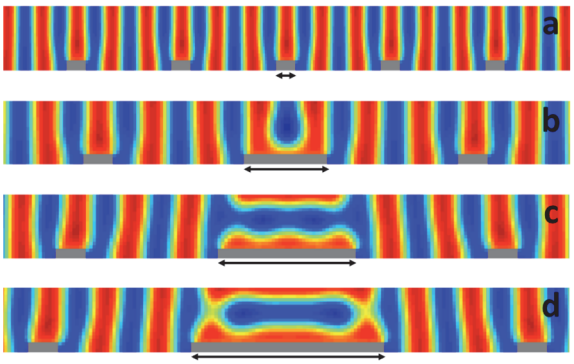

Fig. 6. (Color online) Simulation results for the self-assembled morphology of symmetric *AB* diblock copolymers on the pre-patterned surface ($\phi_{AS} = 0.7$): (a) $W = 0.5\ L_0$, (b) $1.5\ L_0$, (c) $2.5\ L_0$, and (d) $3.5\ L_0$. The size of *W* is denoted by the double-sided arrow. The top-down images corresponding to Figs. 6b-6d are shown in Figs. 5d-5f, respectively. The same coloring was used as in Fig. 3; the *A*-rich and *B*-rich domains are shown by red and blue colors, respectively.

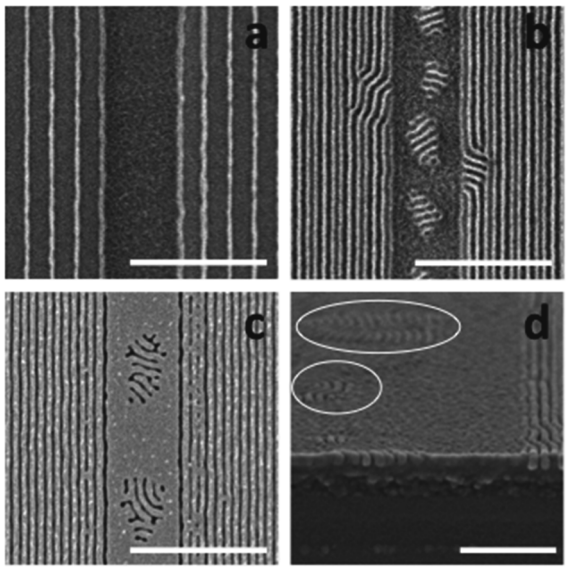

Fig. 7. SEM images of the defects formed on the non-periodic pattern ($W \approx 300$ nm) taken after (a) guide RIE, (b) removal of PMMA, and (c) final pattern transfer to the Si substrate. (d) The tilted cross-sectional SEM image of the self-assembled morphology on a wider non-periodic pattern ($W \approx 978$ nm) after removal of the PMMA. The scale bar (white line) is 500 nm in Fig. 7a-7c and 300 nm in Fig. 7d.

4. Conclusion

In our previous study [11], we have demonstrated an alternative DSA flow that may include non-periodic patterns between the globally aligned DSA lamellae, by using a relatively simple and cost-effective approach. In this work, we investigated how the width of the non-periodic pattern, *W*, would affect on the self-assembled morphology of the symmetric PS-*b*-PMMA, by conducting some experiments and simulations. The experimental results showed that the horizontal lamella was formed on the non-periodic pattern at $W \geq 2.50\ L_0$ (45 nm), and that it was successfully transferred to the Si substrate as a wide line. On the other hand, at $W = 1.5\ L_0$ (30 nm), the non-periodic region was found to be a space on the Si substrate. Our simulation results revealed that the perpendicular lamellae were formed on the non-periodic pattern at $W = 1.5\ L_0$, but the PS-rich domain was not attached to the guide surface; it might be taken off during the removal of PMMA. For $W > 3.5\ L_0$, some large defects were observed in the non-periodic region in the experiments, possibly due to some residues of the neutral materials on top of the non-periodic guide pattern. In order to

obtain a reasonable process window of the DSA flow demonstrated in this study, further improvements will be required for 1) protection of the non-periodic patterns from the neutral layer deposition and 2) more accurate control on the shape of the guide patterns at the boundary between the periodic and non-periodic regions.

Acknowledgements

In this research work we used the supercomputer of ACCMS, Kyoto University.

References

1. R. Gronheid and P. F. Nealey, "*Directed Self-assembly of Block Co-polymers for Nano-manufacturing,*" Elsevier, Oxford, 2015.
2. H. Pathangi, M. Stokhof, W. Knaepen, V. Vaid, A. Mallik, B. T. Chan, N. Vandenbroeck, J. W. Maes, R. Gronheid, *Proc. SPIE*, **9779** (2016) 97791Z.
3. M. Neisser and S. Wurm, *Adv. Opt. Technol.*, **4** (2015) 235.
4. H. Tsai, J. W. Pitera, H. Miyazoe, S. Bangsaruntip, S. U. Engelmann, C.-C. Liu, J. Y. Cheng, J. J. Bucchignano, D. P. Klaus, E. A. Joseph, D. P. Sanders, M. E. Colburn, M. A. Guillorn, *ACS Nano*, **5** (2014) 5227.
5. S. Sayan, B. T. Chan, R. Gronheid, F. V. Roey, M.-S. Kim, L. Williamson, and P. F. Nealey, *Proc. SPIE*, **9051** (2014) 90510M.
6. S. Sayan, T. Marzook, B. T. Chan, N. Vandenbroeck, A. Singh, D. Laidler, E. A. Sanchez, P. Leray, P. R. Delgadillo, R. Gronheid, G. Vandenberghe, W. Clark, A. Juncker, *Proc. SPIE*, **9779** (2016) 97790R.
7. G. S. Doerk, J. Y. Cheng, C. T. Rettner, S. Balakrishnan, N. Arellano, D. P. Sanders, *Proc. SPIE*, **8680** (2013) 86800Y.
8. G. S. Doerk, J. Y. Cheng, G. Singh, C. T. Rettner, J. W. Pitera, S. Balakrishnan, N. Arellano, D. P. Sanders, *Nat. Commun.*, **5** (2014) 5805.
9. Y. Seino, Y. Kasahara, H. Sato, K. Kobayashi, H. Kubota, S. Minegishi, K. Miyagi, H. Kanai, K. Kodera, N. Kihara, Y. Kawamonzen, T. Tobana, M. Shiraishi, S. Nomura, T. Azuma, *Proc. SPIE*, **9423** (2015) 942316.
10. Y. Seino, Y. Kasahara, H. Sato, K. Kobayashi, K. Miyagi, S. Minegishi, K. Kodera, H. Kanai, T. Tobana, N. Kihara, T. Fujiwara, N. Hirayanagi, Y. Kawamonzen, T. Azuma, *Microelectron. Eng.*, **134** (2015) 27.
11. A. Yoshida, K. Yoshimoto, M. Ohshima, K. Kodera, Y. Naka, H. Kanai, S. Kobayashi, S. Maeda, P. Jiravanichsakul, K. Kobayashi, H. Aoyama, *Proc. SPIE*, **9777** (2016) 97771O.
12. T. Ohta and K. Kawasaki, *Macromolecules*, **19**, 2621 (1986).
13. K. Yoshimoto and T. Taniguchi, *J. Photopolym. Sci. Technol.,* **26** (2013) 809.
14. K. Yoshimoto, K. Fukawatase, M. Ohshima, Y. Naka, S. Maeda, S. Tanaka, S. Morita, H. Aoyama, S. Mimotogi, *J. Micro/Nanolith. MEMS MOEMS,* **13** (2014) 031305.